ELSEVIER

Journal of Electroanalytical Chemistry 448 (1998) 163–171

JOURNAL OF ELECTROANALYTICAL CHEMISTRY

Effect of particle size on the electrocatalysis by carbon-supported Pt electrocatalysts: an in situ XAS investigation [1]

Sanjeev Mukerjee, James McBreen *

Department of Applied Science, Brookhaven National Laboratory, Upton, NY 11973, USA

Received 1 November 1996

Abstract

In situ X-ray absorption studies were done in 1 M $HClO_4$, with and without 0.3 M MeOH, on several well-defined carbon-supported Pt electrocatalysts with particle sizes in the range of 25 to 90 Å. Data were obtained at several potentials in the range of 0.0 to 1.14 V vs. RHE. The results show that as the particle size is reduced below 50 Å, the strength of adsorption of H, OH and C_1, moieties such as CO is increased. The strong adsorption of OH explains the reduced specific activity for oxygen reduction on small particles. The reduced activity for methanol oxidation on the small particles is due to a combination of the increased strength of adsorption of both CO and OH. The strong adsorption of H at negative potentials on small Pt particles is sufficient to induce reconstruction and morphological changes in the Pt particles. Both XANES and EXAFS data on a 53 Å particle at 0.84 V indicate that formation of PtOH is the rate determining step in the oxidation of methanol. All these affects are due to an increase in the number of Pt sites with low coordination on the small particles.

Keywords: Carbon-supported Pt; Electrocatalysis; Particle size; X-ray absorption spectroscopy; Methanol oxidation

1. Introduction

The effect of particle size on the electrocatalytic activity, as defined by its turnover number (activity per surface metal atom) has been of interest for both the oxygen reduction reaction (orr) as well as the methanol oxidation reaction for fuel cell applications. In terms of geometric considerations, conventional carbon-supported Pt electrocatalysts have particle sizes in the range of 25 to 80 Å. In this range of particle sizes, there are significant variations, not only in the number of surface to bulk atoms but also in the atoms with different coordination numbers. A detailed description of these geometric characteristics vis à vis particle size is given by Kinoshita [1,2]. For these, the most widely used cluster model is the cuboctahedron. Analysis by Kinoshita based on initial calculations by van Hardeveld and co-workers [3,4] shows that maximum changes occur for sites with ⟨111⟩, ⟨100⟩ crystal planes and those sites which exist at the edge and kink positions of the cluster. While the number of edge and kink sites (low coordination sites) undergo an exponential decrease going from 10 to 90 Å, the sites with ⟨100⟩, ⟨111⟩ showed a reverse effect.

Correlation of these geometric considerations with the results of the effect of particle size on the orr has been reviewed extensively by Kinoshita [1,2], Mukerjee [5] and Stonehart [6]. The fact that particle size effects the kinetics of the orr is supported by a large number of steady state measurements in several electrolytes. The general consensus based on a wide variety of electrocatalysts using different carbon supports, methods of preparation, pretreatments, etc., indicates that ORR does exhibit a particle size effect and that there is a broad maxima in the specific activity for ORR for the particle size range of 35 to 60 Å. The model presented by Kinoshita [1,2] is based on the correlation of this behavior and changes in the availability of low coordination sites relative to those with ⟨111⟩ and ⟨100⟩ crystal planes. This explanation by Kinoshita is significant in the light of the various pathways for oxygen reduction in acid electrolytes (as suggested by Yeager [7,8]), which shows a strong susceptibility of site geometry (average coordination number) based on the particle size. While the correct site geometry is essential for the kinetics of the most widely accepted rate limiting step $* + O_2 +$

* Corresponding author. E-mail: MCBREEN@BNLARM.BNL.GOV.

[1] Dedicated to Aleksandar R. Despic on the ocasion of his seventieth birthday.

0022-0728/98/$19.00

$H^+ + e^- \rightarrow [HO_2]_{ads}$ [9,10] (where $*$ is a Pt site), the strength and susceptibility of the surface oxygenated species also play an important role in determining the overall orr activity. Previous results by Peuckert et al. [11] and Takasu et al. [12] based on cathodic branches of the oxygen reduction peaks indicate higher susceptibility of Pt with smaller particle size towards adsorption by oxygenated species. These results are also supported by XPS results of Parmigiani et al., based on the interaction of oxygen with Pt particles sputtered on Teflon [13]. Besides these there is a wealth of data from gas phase studies on Pt catalysts [14,15] which also supports these observations.

Recent investigations have also shown similar particle size effects on methanol oxidation [16,17]. Unlike oxygen reduction there is a lack of extensive steady state measurements, but the effects can be clearly seen in dynamic measurements. These studies confirm those published earlier by Attwood et al. [18] who found an optimum specific activity for Pt with particle size of 30 Å. Recent reports [16,17] also show a sharp decline in specific activity below 45 Å, activity approaches a limiting value close to twice that on smooth Pt above 50 Å. No clear explanation has, however, emerged to explain these results. However, the general conjecture is that smaller particle sizes (< 50 Å) possess enough low coordination sites to cause strong Pt–OH bonds with high coverage. This results in an unfavorable OH/methanolic residue coverage ratio. A higher number of low coordination sites in small particle sizes may also be unfavorable for adsorption of methanolic species. A recent report by Christensen et al. [19] has pointed to the effects of edge, kink and other low coordination sites in the formation and migration of species such as the linearly bonded CO during methanol oxidation. The exact role of the geometric parameters and interplay of the changes in the electronic structure due to specific adsorbents such as hydrogen, oxygenated species (OH), CO, methanol, etc., however, remains unclear.

X-ray absorption spectroscopy (XAS) offers the ability to probe simultaneously changes in the electronic and geometric parameters of supported Pt under in situ electrochemical conditions with element specificity. The ability to probe the L absorption edges (p–d transitions) of the Pt under in situ conditions using the near edge part of the spectra (X-ray absorption near edge structure, XANES) provides a direct measure of Pt 5d-band vacancies/atom. The post-edge region of the spectrum (up to 1500 eV beyond the L_3 edge, referred to as the extended X-ray absorption fine structure, EXAFS) provides a simultaneous measure of the changes in the nearest neighbor interactions of Pt (bond distances and coordination number). The aim of this investigation therefore was to conduct such an in situ XAS investigation on a series of Pt + C electrocatalysts with well-defined particle sizes. The objective was to first investigate the electrocatalysis of Pt as a function of particle size in 1 M $HClO_4$, followed by a similar study under conditions of methanol oxidation.

2. Experimental

A series of carbon-supported Pt electrocatalysts with a Pt loading in the range of 20 to 60% were procured from ETEK Inc. (Natick, MA). These correspond to particle sizes in the range of 25 to 90 Å as per manufacturers specifications [2]. These particle sizes were independently verified using X-ray diffraction line broadening analysis (Scherrer equation). The X-ray diffraction data was acquired at beam line X-27A of the National Synchrotron Light Source (NSLS). Details of the beam line set up, resolution, etc., are given elsewhere [20]. In situ XAS analysis was carried out in 1 M $HClO_4$, an electrolyte of choice due to its low X-ray absorption characteristics and non-interference due to lack of anion adsorption (unlike the anions of H_2SO_4 or H_3PO_4). XAS investigations were carried out at the NSLS at beam line X23A2. Measurements were made in the transmission mode at the Pt L_3 and L_2 edges at potentials of 0.0, 0.24, 0.54, 0.84 and 1.14 V vs. RHE, in a series of experiments with and without 0.3 M MeOH in the electrolyte. Details of the electrode preparation, spectro-electrochemical cell, beam line configuration, monochromator design, resolution, etc., are provided in detail elsewhere [21,22]. All electrodes were soaked in 1 M $HClO_4$ for 48 h prior to incorporation into the spectro-electrochemical cell, to ensure a totally flooded environment, an essential requirement since XAS is a bulk averaging technique. Potential control was provided by a Princeton Applied Research (PAR, model 273) potentiostat interfaced with an IBM PS/2 computer. The reference electrode was a sealed hydrogen electrode, hence all potentials in this paper are vs. RHE. The sweep rate used for the potential transitions was $2\,mV\,s^{-1}$. All measurements were done in the transmission mode with three ionization chamber detectors (incidence (I_o), transmittance (I_t) and reference (I_{ref})). The reference channel (Pt foil) was used for internal calibration of edge positions.

Details of the methodology used for the XANES and EXAFS analysis are given in refs. [22,23]. The Pt 5d-band vacancies were determined from the Pt L_3 and L_2 XANES following the methodology developed by Mansour [24], details of which are given elsewhere [22]. Details of the methodology used for the EXAFS analysis are given elsewhere [22]. For detailed EXAFS analysis, phase and amplitude parameters for Pt–O and Pt–Pt interactions were obtained using the liquid N_2 EXAFS data for a Pt foil (5 μm) and $Na_2Pt(OH)_6$ reference standards.

3. Results and discussion

Table 1 lists all the electrocatalysts in terms of their Pt loading and the corresponding particle size based on X-ray

[2] Particle size obtained using TEM, personal communication.

Table 1
Calculated values of the effect of particle size on ratio of surface to total number of atoms and the coordination numbers for cubo- and icosa-hedron models for Pt clusters

Pt loading on carbon/%	Particle size XRD analysis ([111] line at FWHM)/Å	Ns/Nt[a]	$N_{\text{cubo-octahedral}}$	$N_{\text{icosahedral}}$
20	30	37.52	10.35	10.62
30	40	28.77	10.79	11.05
40	53	21.56	11.12	11.22
60	90	11.31	11.45	11.53

[a] This ratio is the same for both cuboctahedron and icosahedron models.

diffraction line broadening analysis at full width at half maximum (FWHM). For this purpose the broadening of the ⟨111⟩ diffraction line was used. In order to correlate these particle sizes with geometric parameters such as the ratio of surface to bulk atoms, average coordination numbers (cuboctahedron model), sites with lower coordination numbers, etc., algorithms based on methodologies developed by Benfield [25] were used. These algorithms are based on original calculations by van Hardeveld and coworkers [3,4] and use concentric shells of atoms in model systems such as the cuboctahedron system. Based on these algorithms some of the geometric parameters have been calculated as shown in Table 1. The advantage of these algorithms is that they permit calculations of the mean nearest neighbor coordination number of atoms in the cluster which corresponds to those obtained from the nearest neighbor interactions in EXAFS analysis. Table 1 shows these values for both cuboctahedron as well as for the related cluster geometry of an icosahedron. As evident from the values in Table 1, the geometric parameters from the two structures approach each other closely beyond 70 Å; below 40 Å, however, the structures exhibit greater differences in the coordination numbers.

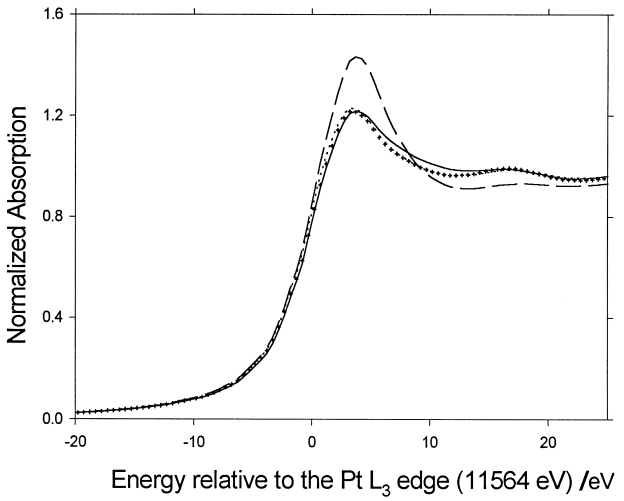

Fig. 1. XANES at the Pt L_3 edge for Pt+C (30 Å) in 1 M $HClO_4$ as a function of potential vs. Pt reference foil (+). 0.0 V (————), 0.54 V (· · ·) and 0.84 V (— — —)

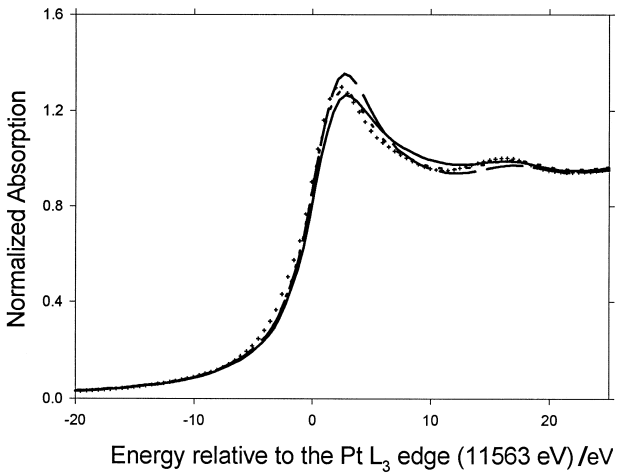

Fig. 2. XANES at the Pt L_3 edge for Pt+C (53 Å) in 1 M $HClO_4$ as a function of potential vs. Pt reference foil (+). 0.0 V (————), 0.54 V (· · ·) and 0.84 V (— — —).

3.1. XAS results in 1 M $HClO_4$

Fig. 1 shows the XANES at the Pt L_3 edge for Pt + C (30 Å) electrocatalyst in 1 M $HClO_4$. The spectra show that at 0.0 V there is considerable widening in the white line near the high energy side of the peak at (5 to 15 eV). At 0.54 V (double layer region) the spectra for Pt + C is identical to that of the pure Pt reference foil, which indicates that there is no interference due to anion or other adsorption effects such as H or OH. The widening of the white line at 0.0 V has been discussed in detail in a previous publication [26]. This widening is ascribed to transitions into empty Pt–H anti-bonding orbitals. Such

Table 2
Calculated Pt 5d-band vacancy/atom from analysis of L_3 and L_2 white lines as a function of potential for Pt+C electrocatalysts with different particle size in 1 M $HClO_4$

Particle size/Å	Pt d-band vacancy/atom		
	0.0 V	0.54 V	0.84 V
30	0.345	0.329	0.377
40	0.341	0.330	0.365
53	0.333	0.329	0.342
90	0.328	0.327	0.331

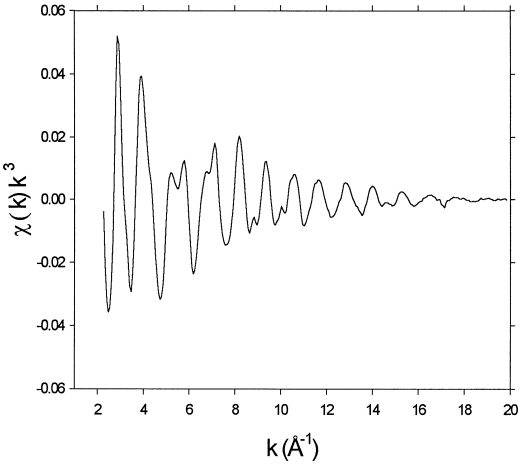

Fig. 3. EXAFS at the Pt L_3 edge for Pt + C (90 Å) in 1 M $HClO_4$ at 0.0 V vs. RHE.

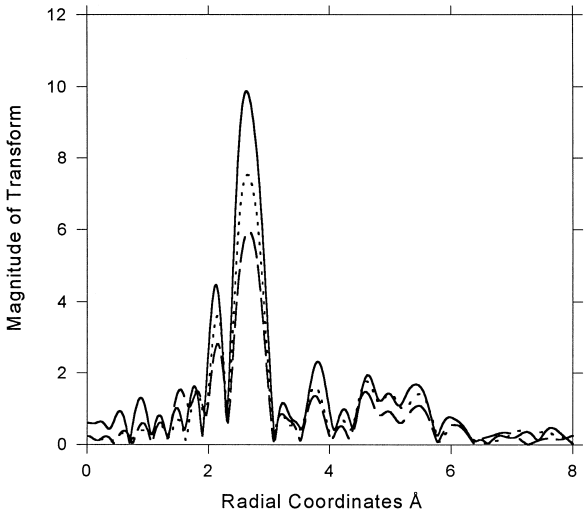

Fig. 4. Fourier transforms at the Pt L_3 edge for Pt + C (30 Å) in 1 M $HClO_4$ at 0.0 V (————), 0.54 V (· · ·) and 0.84 V (— — —) vs. RHE.

widening of the white line has been reported before both in the gas phase as well as under electrochemical conditions [22,24,26,27] and the interpretation is based on a suggestion by Samant and Boudart [28]. At 0.84 V there is a considerable increase in the white line which has been shown to be due to the adsorption of oxygenated species [22]. Comparison of the corresponding XANES spectra for Pt + C (53 Å) (Fig. 2) shows that the widening of the white line at 0.0 V is reduced and that there is a great reduction in increase of the white line intensity at 0.84 V. Corresponding values of the Pt 5d-band vacancies/atom (Table 2) reflect these observations as a function of particle size. These effects on the XANES spectra at different potentials were completely reversible.

The EXAFS at the Pt L_3 edge was used to probe changes in the short-range atomic order around Pt as a function of particle size at different potentials. Fig. 3 shows the representative plot of the raw EXAFS (k^3 weighted) at the Pt L_3 edge for Pt + C (90 Å) at 0.0 V in 1 M $HClO_4$. As evident from the figure, the quality of the in situ EXAFS data is good and the modulation stretched as far as $k = 17\,Å^{-1}$. Fig. 4 shows the forward Fourier transforms of the EXAFS spectrum for Pt + C (30 Å) as a function of potential. The windows in *k*-space used for obtaining the Fourier transforms are given in Table 3 and for the reference standard in Table 4. The higher magnitude of the Fourier transform at 0.0 V indicates a significant change in the structural parameters for the Pt + C electrocatalyst in the hydrogen region relative to the double layer (0.54 V). This observation of a higher magnitude of the Fourier transform is in agreement with previously reported in situ results on a supported Pt + C electrocatalyst [29]. The increase in the magnitude of the first peak in the Fourier transform could be attributed to changes in the Pt–Pt coordination number *N*, changes in the Debye–Waller factor $\Delta\sigma^2$, the introduction of another coordination shell (e.g. Pt–C) or to forward scattering effects due to hydrogen in the Pt lattice. However, recently published results [26] show that the primary contributor to this effect is a change in coordination number. This indicates a possible change in particle morphology such as that from a sphere to a plane raft-like configuration during the potential transition from 0.0 to 0.54 V. The potential shift to 0.84 V shows a lowering of the magnitude of the Pt–Pt interactions due to adsorption of oxygenated species and the rise of an extra peak at 1.5 Å due to Pt–O interactions. The corresponding Fourier transforms for Pt + C (53 Å) (Fig. 5) show a significant reduction in the change of Pt–Pt interactions while going from 0.0 to 0.54 V. This

Table 3
Fourier transformation ranges for the forward and inverse transforms (k^3 weighted) for Pt + C electrocatalysts at various potentials in 1 M $HClO_4$ as a function of particle size.

Particle size/Å	0.0 V		0.54 V		0.84 V	
	Δk/Å^{-1}	Δr/Å	Δk/Å^{-1}	Δr/Å	Δk/Å^{-1}	Δr/Å
30	3.53–14.31	1.41–3.41	3.49–14.23	1.40–3.05	3.26–14.15	1.30–3.04
40	2.73–15.61	1.48–3.50	2.73–15.61	1.40–3.54	2.76–15.56	1.20–3.05
53	2.90–15.56	1.58–3.58	2.8–15.56	1.48–3.52	2.75–15.50	1.10–3.12
90	2.73–15.54	1.52–3.40	2.73–15.54	1.42–3.52	2.73–15.54	1.12–3.12

Table 4
Fourier transformation ranges for the forward and inverse transforms (k^3 weighted) for the reference standards

Reference standard	Δk/Å^{-1}	Δr/Å	N_{ref}	R_{ref}
Pt–Pt Pt foil (liq. N_2 temp.)	3.55–19.22	1.04–3.52	12	2.774
Pt–O $Na_2Pt(OH)_6$ (liq. N_2 temp.)	3.52–17.18	1.05–2.40	6	2.052

indicates that for larger particles the changes in the shape and morphology of the particle during this potential transition are much lower. Transition into the oxide-covered region (0.84 V) lowers the magnitude of Pt–Pt interactions.

Detailed EXAFS analysis was performed after obtaining the inverse Fourier transform and performing fits with phase and amplitude parameters derived experimentally from a Pt reference foil (for Pt–Pt interactions) and $Na_2Pt(OH)_6$ (Pt–O interactions) at liquid N_2 temperature. All fits were performed using iterative least squares fitting [30]. All the relevant windows for the inverse transform for the sample and for the reference standard are given in Tables 3 and 4 respectively. The approach taken in fitting the sample data was to choose the simplest model first and attempt to get unique solutions to the fits. For all the Pt + C electrocatalysts best fits were obtained with a single Pt–Pt coordination shell at both 0.0 and 0.54 V. At 0.84 V it was necessary to use a two shell fit with both Pt–Pt and Pt–O coordination shells. Fig. 6 shows representative plots of the quality of these fits in both *k* (Fig. 6(a)) and *r*-space (Fig. 6(b)) for Pt + C (30 Å) at 0.0 V. The EXAFS parameters obtained from this analysis are shown in Table 5. The values for the coordination numbers reflect quantitatively those observed from the forward Fourier transforms (Figs. 4 and 5). Assuming that the shape of the particle at 0.0 V closely resembles those based on the cuboctahedron model, a comparison of the coordination numbers as a function of particle size shows very close agreement with the values in Table 1. Errors in the determination of coordination numbers for single shell fits (as determined using methodology

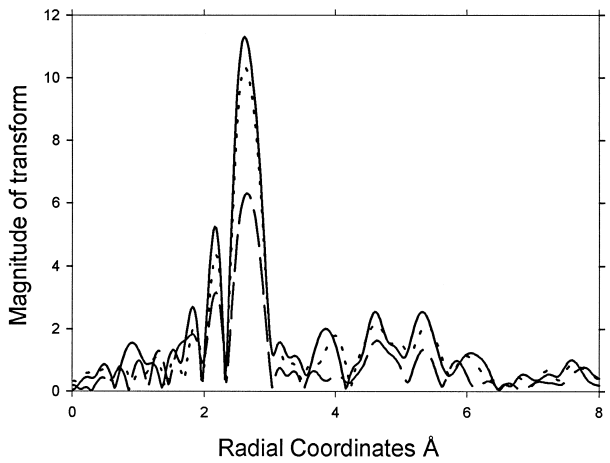

Fig. 5. Fourier transforms at the Pt L_3 edge for Pt+C (53 Å) in 1 M $HClO_4$ at 0.0 V (————), 0.54 V (· · ·) and 0.84 V (— — —) vs. RHE.

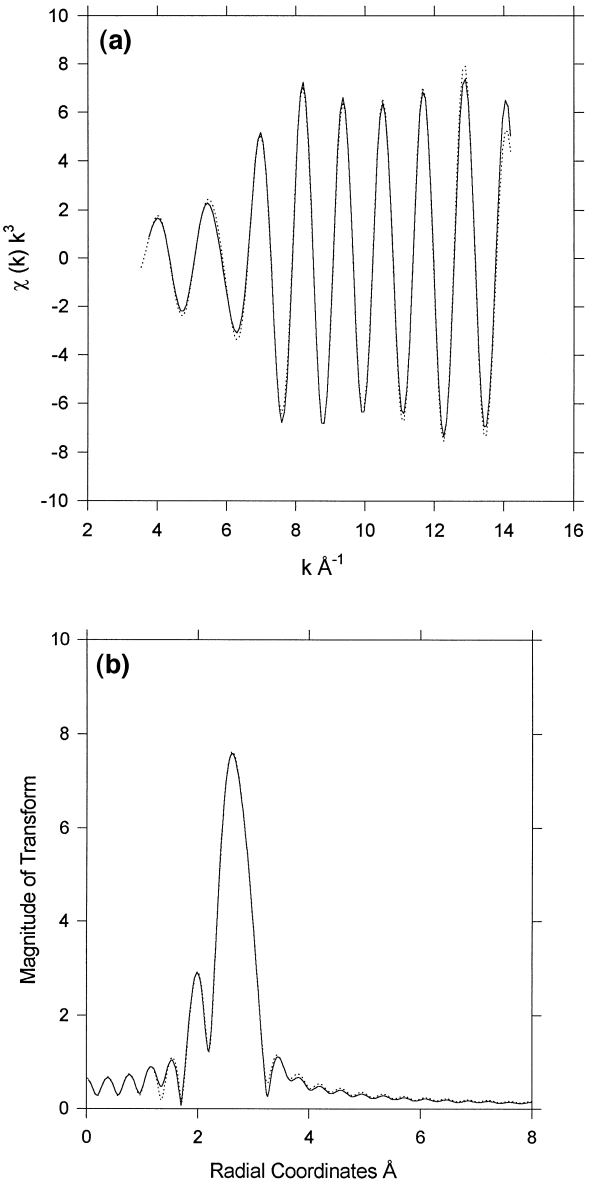

Fig. 6. Single shell fits for Pt+C (30 Å) in 1 M $HClO_4$ at 0.0 V vs. RHE in (a) *k*-space and (b) *r*-space. The fits are k^3 weighted for the sample data denoted by (· · ·) and the fitted data (————).

described elsewhere [31]) ranged between 1 to 8% and 0.005 to 0.01 Å for *R*. For two shell fits, these limits were typically in the range of 5 to 14% for *N* and 0.007 to 0.012 Å for *R*. Hence, due to the limits of error inherent in the determination of the coordination numbers it was not possible to differentiate between the cuboctahedron and icosahedron models.

Since the broadening of the L_3 white line at 0.0 V is due to adsorbed H and the increase of the white line at 0.84 V is due to adsorbed OH, comparison of the effect of various particle sizes must be normalized with respect to the fraction of surface Pt atoms. Fig. 7 shows a normalized plot of the change in d-band vacancy/atom on going from 0.54 to 0.0 V. The changes increased as the particle size

Table 5
Structural parameters obtained from the analysis of in situ EXAFS at the Pt L_3 edge for Pt + C electrocatalysts of different particle size as a function of potential in 1 M $HClO_4$

Particle size/Å	Coordination shell	0.0 V				0.54 V				0.84 V			
		N	R/Å	$\Delta\sigma^2$/Å^2	ΔE_o/eV	N	R/Å	$\Delta\sigma^2$/Å^2	ΔE_o/eV	N	R/Å	$\Delta\sigma^2$/Å^2	ΔE_o/eV
30	Pt–Pt	10.56	2.772	0.0044	0.93	8.66	2.773	0.0044	−0.88	6.73	2.773	0.0048	−0.20
	Pt–O									1.69	2.037	0.0042	2.48
40	Pt–Pt	10.96	2.768	0.0048	−0.25	9.55	2.776	0.0043	−2.78	7.75	2.774	0.0049	−0.86
	Pt–O									3.24	2.056	0.0051	3.68
53	Pt–Pt	11.15	2.770	0.0043	−0.13	10.63	2.773	0.0045	−0.61	8.05	2.776	0.0042	−2.91
	Pt–O									3.06	2.100	0.0075	−6.24
90	Pt–Pt	11.47	2.774	0.0038	0.36	11.32	2.776	0.0037	−0.27	10.42	2.775	0.0034	−1.14
	Pt-O									1.05	2.073	0.0086	5.87

was reduced from 70 to 30 Å. Fig. 8 shows the corresponding normalized plot for the change in d-band vacancy on going from 0.0 to 0.84 V. Again the changes increase with decreasing particle size. The results indicate that the electronic effects due to adsorption of H and OH are larger for the small particles even when the results are normalized to account for the number of surface atoms. This indicates stronger adsorption of both H and OH on the smaller particles.

Our previous work on 30 Å Pt + C particles showed that potential excursions from 0.54 to 0.0 V induced morphological changes in the Pt particles. These result in changes in the Pt–Pt coordination number N. This was ascribed to electrochemically induced restructuring of the small Pt particles at negative potentials. On going to 0.54 V the reconstruction is lifted. Fig. 7 also shows a plot of the change in the Pt–Pt coordination number ΔN for the various Pt particle sizes. In the case of the small particles, strong absorption of H induces morphological changes in the Pt clusters that are reflected in the increased Pt–Pt coordination numbers. For particle sizes above 50 Å, there are no changes in the Pt–Pt coordination number. For the larger particle sizes the Pt approaches the case of bulk Pt single crystals, where surface relaxation [32], but no reconstruction [33], is observed at negative potentials.

Both XANES and EXAFS results therefore confirm the stronger adsorption of H and OH on smaller particles. The strong adsorption of OH in the oxygen reduction region can account for the decline in specific activity for oxygen reduction on these small particles, as shown previously by Kabbabi et al. [17] on the same electrocatalysts (ETEK Inc.) within the same particle size range.

3.2. XAS in 1 M $HClO_4$ + 0.3 M MeOH

Fig. 9 shows the XANES at the Pt L_3 edge for Pt + C (30 Å) in 1 M $HClO_4$ + 0.3 M MeOH. At 0.0 V there is a small widening of the white line, similar to that observed in 1 M $HClO_4$. However, the magnitude of this widening is significantly lower than that observed without MeOH, and can be attributed to the adsorption of organic species on the surface such as methanoxy and aldehydic moieties.

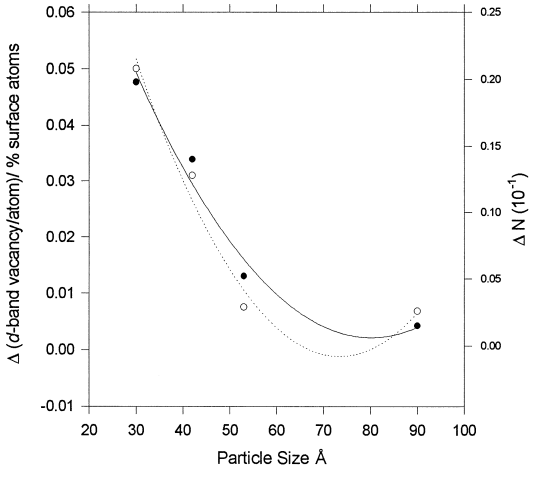

Fig. 7. The effect of particle size on the change in the normalized d-band vacancies (d-band vacancies/% surface atoms) (· · ·) in going from 0.54 to 0.0 V. The change in the Pt–Pt coordination number, as determined from L_3 EXAFS, is also shown (————).

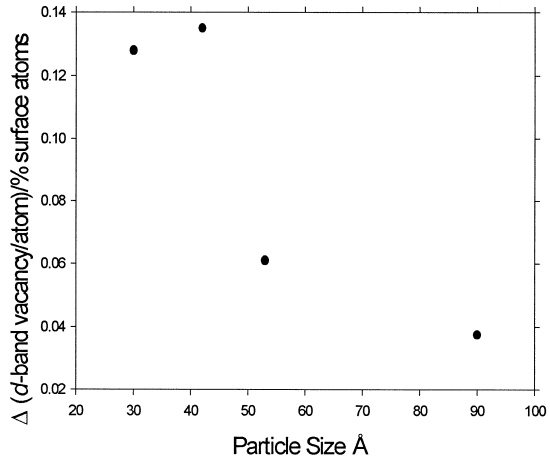

Fig. 8. Variation of d-band vacancies per percent surface atoms between 0.54 and 0.84 V in 1 M $HClO_4$ as a function of particle size.

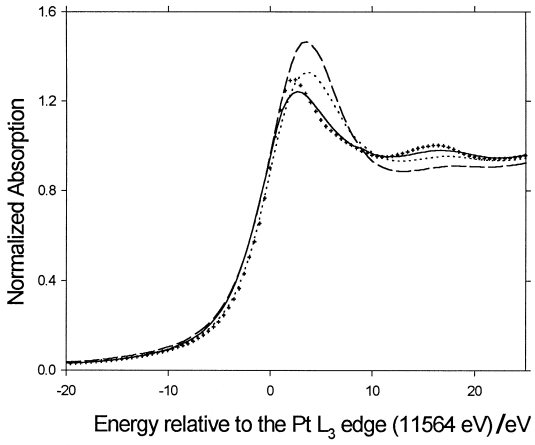

Fig. 9. XANES at the Pt L_3 edge for Pt + C (30 Å) in 1 M $HClO_4$ + 0.3 M MeOH as a function of potential vs. Pt reference foil (+). 0.0 V (————), 0.54 V (· · ·) and 0.84 V (— — —) vs. RHE.

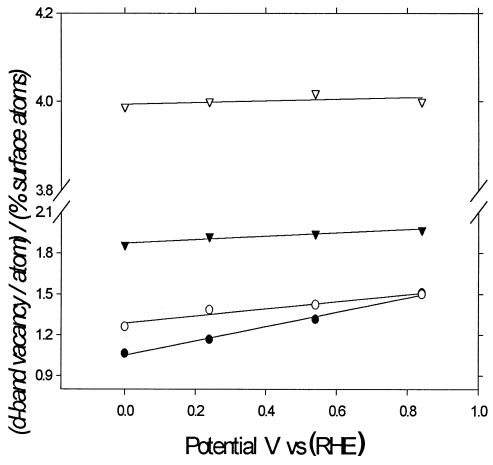

Fig. 11. Variation of d-band vacancy per percent surface atom as a function of potential in 1 M $HClO_4$ + 0.3 M MeOH for particle sizes 30 Å (●), 42 Å (○), 53 Å (▼) and 90 Å (▽).

Such a mixed adsorption effect has been previously reported for Pt using electrochemical mass spectrometry [34] and the electrochemical quartz crystal microbalance [35]. However, a direct correlation with these previous investigations is difficult due to their use of unsupported Pt electrocatalysts. It is, however, evident that the effect of hydrogen bonding is significantly lowered in the presence of methanol for the 30 Å particles at this potential. At 0.54 V there is a significant increase in the white line which can be attributed primarily to CO adsorption and the onset of its oxidation. This fact was confirmed independently by Pt L_3 XANES on the Pt + C electrocatalyst after CO adsorption [36]. At 0.84 V the increase in the intensity of the white line is similar to that in 1 M $HClO_4$. There is a further increase in this white line intensity at 1.14 V (not shown). Pt L_3 XANES at 0.4 V following the cathodic branch of the return sweep shows spectra exactly matching those observed initially at 0.0 V (not shown), thereby indicating the complete reversibility of these observed processes. Comparison of these effects with Fig. 10 shows that the XANES for the 53 Å Pt + C exhibits very different behavior. At 0.0 V there is significant widening of the white line, which in light of the previous results can be attributed to the mixed effect of hydrogen adsorption and formation of CO on the Pt surface. At 0.54 V the widening of the white line shows a slight increase, indicating a build-up of CO species on the surface. However, comparison with the spectra at the corresponding potential for the 30 Å particle shows that perturbation of the Pt 5d-band electronic states is significantly lower for the larger particle. Similarly, at 0.84 V, comparison of the white line intensities for the 30 and 53 Å particles shows significantly lower white line intensities for the larger particle. Fig. 11 summarizes these effects more quantitatively. The plot of variation of the Pt 5d-band vacancy (normalized with respect to percent surface atoms) as a function of potential

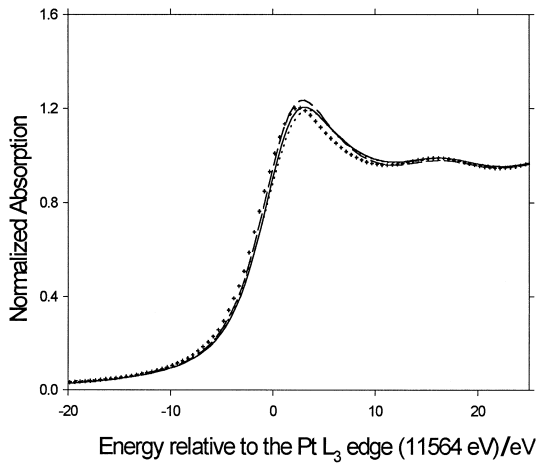

Fig. 10. XANES at the Pt L_3 edge for Pt + C (53 Å) in 1 M $HClO_4$ + 0.3 M MeOH as a function of potential vs. Pt reference foil (+). 0.0 V (————), 0.54 V (· · ·) and 0.84 V (— — —) vs. RHE.

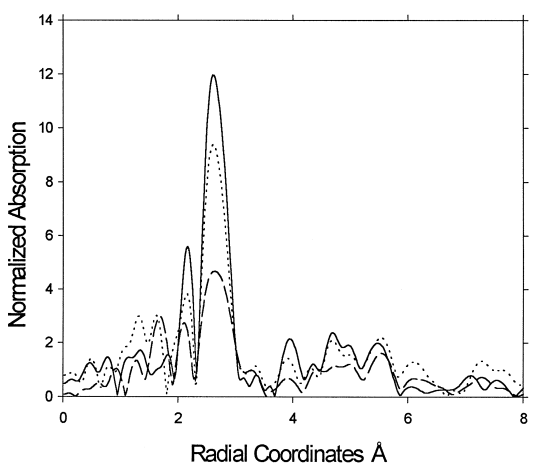

Fig. 12. Fourier transforms at the Pt L_3 edge for Pt + C (30 Å) in 1 M $HClO_4$ + 0.3 M MeOH as a function of potential. 0.0 V (————), 0.54 V (· · ·) and 0.84 V (— — —) vs. RHE.

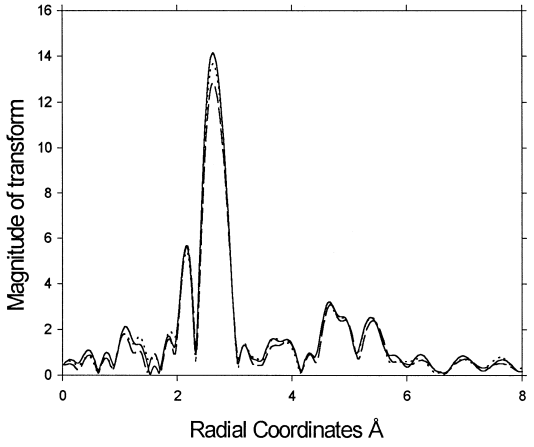

Fig. 13. Fourier transforms at the Pt L_3 edge for Pt+C (53 Å) in 1 M $HClO_4$ + 0.3 M MeOH as a function of potential. 0.0 V (————), 0.54 V (· · ·) and 0.84 V (— — —) vs. RHE.

for Pt with different cluster sizes indicates that, in contrast to particles above 50 Å, the smaller crystallites show increasing susceptibility to perturbation of the Pt 5d electronic states. This directly reflects its susceptibility to form strongly adsorbed species. This result indicates that the smaller particles enhance the absorption of H, OH and CO.

Figs. 12 and 13 show the forward Fourier transforms at the Pt L_3 edge for Pt + C with 30 and 53 Å cluster sizes as a function of potential. For the 30 Å particle, the EXAFS shows well-defined features due to the presence of methanol and its oxidation. Comparison of the Fourier transforms at 0.0 and 0.54 V shows evidence for the onset of a CO adsorption effect at 0.54 V and its relative absence at 0.0 V, as demonstrated by the existence of the extra peaks below 1.8 Å. This interpretation has been confirmed from the corresponding EXAFS spectra for chemisorbed CO on Pt + C [36]. There is also the associated lowering of the magnitude of the Fourier transform at 0.54 V, due to consequent lowering of the Pt–Pt interactions. At 0.84 V there is the expected further decrease in the Pt–Pt interactions and the emergence of the Pt–O peak below 2 Å, which is similar to those observed in 1 M $HClO_4$. For the Pt + C with a 53 Å cluster size, there is very little change in the Fourier transforms as a function of potential. In contrast to the spectra in 1 M $HClO_4$ without methanol (Fig. 5), there is very little evidence of formation of an oxide layer at 0.84 V in the presence of methanol. This therefore confirms the results observed in the Pt L_3 XANES spectra.

A comparison of the data in Figs. 1, 4, 9 and 12 shows that at 0.84 V there is very little difference in the XANES and EXAFS for the 30 Å particle in 1 M $HClO_4$ and 1 M $HClO_4$ + 0.3 M MeOH. However, in the case of the 53 Å particle (Figs. 2, 5, 10 and 13) large differences were observed. In the case of larger particles the adsorbed OH is consumed by the methanol oxidation reaction, indicating that formation of Pt–OH is the rate determining step. This agrees with earlier observations of Gasteiger et al. [37]. In the case of the smaller particles, methanol oxidation seems to be inhibited both by strongly adsorbed OH as well as CO. This is evident from Figs. 7 and 11. Under the conditions of enhanced kinetics on the 53 Å particles, formation of Pt–OH becomes the rate determining step.

It is clear that particle size plays an important role in the adsorption of H, OH and C_1 entities such as CO. All indications are that the adsorption of these species are stronger on the smaller particles (< 50 Å). This is probably due to an increase in the low coordination sites in the small particles. These observations are in agreement with those previously reported for Pt cluster interactions with a zeolite support [38] and gas phase measurements on Pt clusters on an alumina support [39]. The trends observed agree with the conclusions of Kinoshita for oxygen reduction [2] and those of Frelink et al. [16] and Kabbabi et al. [17] (with similar electrocatalysts) for methanol oxidation. This investigation provides the first direct spectroscopic confirmation of the effect of particle size on the electrocatalysis on small Pt particles.

4. Conclusions

In situ XAS studies show that as the particle size of carbon-supported Pt clusters is reduced below 50 Å there is strong adsorption of H, OH and C_1 compounds such as CO. In small particles, H adsorption is sufficiently strong to induce restructuring and morphological changes in Pt clusters at negative potentials. The strong adsorption of OH beyond 0.8 V on small particles (< 50 Å) inhibits the reduction of oxygen. The combined effect of strongly adsorbed CO and OH on these small particles inhibits methanol oxidation.

Acknowledgements

The authors gratefully acknowledge the support of the US Department of Energy, Division of Material Science, Brookhaven National Laboratory (contract # DEACO2-76CH00016) for its role in the development and operation of the National Synchrotron Light Source (NSLS). The help of NIST personnel at the Beam Line X23A2, in particular Joe Woicik and John Kirkland, is gratefully acknowledged. The experimental work at Brookhaven was supported by the Office of Transportation Technologies, Electric and Hybrid Vehicles Division of D.O.E under contract # DEA-CO2-76CH00016.

References

[1] K. Kinoshita, Mod. Aspects of Electrochem. 14 (1982) 557.
[2] K. Kinoshita, J. Electrochem. Soc. 137 (1990) 845.

[3] R. van Hardeveld, F. Hartog, Surf. Sci. 15 (1969) 189.
[4] R. van Hardeveld, A.V. Monfoort, Surf. Sci. 4 (1969) 396.
[5] S. Mukerjee, J. App. Electrochem. 20 (1990) 537.
[6] P. Stonehart, Ber. Bunsenges. Phys. Chem. 94 (1990) 913.
[7] E. Yeager, Electrochim. Acta 29 (1984) 1527.
[8] E. Yeager, J. Mol. Catal. 38 (1986) 5.
[9] A. Damjanovic, V. Brusic, Electrochim. Acta 11 (1967) 615.
[10] A.J. Appleby, J. Electrochem. Soc. 117 (1970) 328; J. Electroanal Chem. 357 (1993) 117.
[11] M. Peuckert, T. Yoneda, R.A. Dalla Betta, M. Boudart, J. Electrochem. Soc. 133 (1986) 944.
[12] Y. Takasu, F. Fujii, K. Yasuda, Y. Iwanaga, Y. Matsuda, Electrochim. Acta 34 (1989) 453.
[13] F. Parmigiani, E. Kay, P.S. Bagus, J. Electron. Spectrosc. Relat. Phenom. 50 (1990) 39.
[14] F.V. Hanson, M. Boudart, J. Catal. 53 (1978) 56.
[15] M. Boudart, D.M. Collins, F.V. Hanson, W.E. Spicer., J. Vac. Sci. Technol. 14 (1977) 441.
[16] T. Frelink, W. Visscher, J.A.R. van Veen, J. Electroanal. Chem. 382 (1995) 65.
[17] A. Kabbabi, F. Gloaguen, F. Andolfatto, R. Durand, J. Electroanal. Chem. 373 (1994) 251.
[18] P.A. Attwood, B.D. McNicol, R.T. Short, J. Appl. Electrochem. 10 (1980) 213.
[19] P.A. Christensen, A. Hamnett, J. Munk, G.L. Troughton, J. Electroanal. Chem. 370 (1994) 251.
[20] T.R. Thurston, N.M. Jisrawi, S. Mukerjee, X.Q. Yang, J. McBreen, M.L. Daroux, X.K. Xing, J. Appl. Phys. Lett. 69 (1996) 194.
[21] J. McBreen, W.E. O'Grady, K.I. Pandya, R.W. Hoffman, D.E. Sayers, Langmuir 3 (1987) 428.
[22] S. Mukerjee, S. Srinivasan, M.P. Soriaga, J. McBreen, J. Electrochem. Soc. 142 (1995) 1409.
[23] J. McBreen, S. Mukerjee, J. Electrochem. Soc. 142 (1995) 3399.
[24] A.N. Mansour, Ph.D. Thesis, University of North Carolina, Raleigh, NC, 1983.
[25] R.E. Benfield, J. Chem. Soc. Faraday Trans. 88 (1992) 1107.
[26] S. Mukerjee, J. McBreen, J. Electrochem. Soc. 143 (1996) 2285.
[27] A.N. Mansour, J.W. Cook Jr., D.E. Sayers, R.J. Emrich, J.R. Katzer, J. Catal. 89 (1984) 464.
[28] M.G. Samant, M. Boudart, J. Phys. Chem. 95 (1991) 4070.
[29] P.G. Allen, S.D. Conradson, M.S. Wilson, S. Gottesfeld, I.D. Raistrik, J. Valerio, M. Lovato, Electrochim. Acta 39 (1994) 2415.
[30] G.H. Via, J.H. Sinfelt, F.W. Lytle, J. Chem Phys. 71 (1979) 690.
[31] B.K. Teo, EXAFS: Basic Principles and Data Analysis (Inorganic Chemistry Concepts 9), Springer, 1986, p. 132.
[32] I.M. Tidswell, N.M. Markovic, P.N. Ross, Phys. Rev. Lett. 71 (1993) 1601.
[33] M.S. Zei, N. Batina, D.M. Kolb, Surf Sci. Lett. 306 (1994) L519.
[34] M. Krausa, W. Vielstich, J. Electroanal. Chem. 379 (1994) 307.
[35] C.P. Wilde, M. Zhang, Electrochim. Acta 39 (1994) 347.
[36] J. McBreen, S. Mukerjee, Extended Abstr. 190th Meet. of the Electrochemical Society, San Antonio, TX, October 6–11, 1996.
[37] H.A. Gasteiger, N.M. Markovic, P.N. Ross Jr., E.J. Cairns, J. Phys. Chem. 97 (1993) 12020.
[38] M.G. Samant, M. Boudart, J. Phys. Chem. 95 (1994) 4070.
[39] J.H. Sinfelt, G.D. Meitzner, Acc. Chem. Res. 26 (1993) 1.